International Journal of Mechanical and Electrical Engineering
ISSN: 3005-9615 (Print), ISSN: 3005-7132 (Online) | Volume 5, Number 3, Year 2025
DOI: https://doi.org/10.62051/ijmee.v5n3.07
Journal homepage: https://wepub.org/index.php/IJMEE/index

Design and Analysis of Three-Degree-of-Freedom Nanopositioning Platform

Shiwen Hong [1], Haonan Zhu [1], Zhina Lv [1], Liangyu Cui [1, 2, *]

[1] School of Mechanical Engineering, Tianjin University of Technology and Education, Tianjin, China
[2] Tianjin Key Laboratory of High Performance Manufacturing Technology & Equipment, Tianjin, China
* Corresponding Author: Liangyu Cui

ABSTRACT

To address the issue that the ultra-precision positioning device in the form of piezoelectric ceramic actuated flexible hinge can only be positioned in a single direction, a three-degree-of-freedom nano-positioning platform is proposed. Firstly, the structural designs of the flexible hinge guiding mechanism and the flexible hinge transmission amplification mechanism are conducted, and then the overall structural model of the three-degree-of-freedom nano-positioning platform is designed. Through the static and dynamic modeling, analysis and verification of the bridge amplification mechanism, a theoretical basis is provided for the design of the bridge amplification mechanism. Subsequently, the dynamic platform is simulated, analyzed and verified using ANSYS Workbench to further validate the rationality of the design.

KEYWORDS

Nano Positioning Platform; Flexible Hinge; Amplification Mechanism.

1. INTRODUCTION

With the rapid development of nanotechnology applications and the gradual deepening of analysis and research in the micro-distribution world, the requirement for the accuracy of nano-positioning has become increasingly stringent. Against this backdrop, nano-positioning application technology has emerged and plays a pivotal role in the scientific manufacturing and scientific analysis, primarily contributing to the enhancement of positioning precision and recognition rate. Nowadays, nano-positioning technology has been widely applied in various fields, including optical engineering, ultra-precision machining [1], life sciences, semiconductor manufacturing [2], micro-manipulation [3], and scanning tunneling microscopy [4]. To accommodate the ultra-precision positioning in different scenarios, nano-positioning platforms must possess the capability for multi-directional positioning.

Piezoelectric ceramic actuator-driven flexible hinge mechanisms for ultra-precision positioning devices can only achieve unidirectional positioning; multi-directional positioning can only be achieved by stacking individual unidirectional positioning devices, which results in cumulative errors and complex structures. To achieve multi-directional positioning, researchers have proposed various methods. Zhou Liping et al. designed a planar 3-PRR micro-motion platform driven by a linear ultrasonic motor [5], employing visual positioning for closed-loop control, with a workspace of 60mm×60mm×20° and a control precision of only 5μm; however, it uses a branched structure, resulting in a larger overall structure. Meng Fuanxun [6] et al. designed a planar three-degree-of-freedom micro-displacement parallel flexible positioning platform driven by piezoelectric ceramics. This micro-displacement positioning platform possesses both large stroke and high precision,

compensating for the current deficiencies in micro-displacement positioning platforms. Tian Yanling [7] et al. designed a three-degree-of-freedom micro-positioning platform for nano-positioning and dynamic compensation of vibration errors.

To overcome the limitations of unidirectional positioning, this paper proposes a three-degree-of-freedom nano-positioning platform. The platform includes the structural design of flexible hinge guidance and transmission amplification mechanisms, as well as the overall structural model. The design is validated through static and dynamic modeling analysis of the bridge-type amplification mechanism. Simulations of the moving platform using ANSYS Workbench further confirm the rationality of the design.

2. ORGANIZATION OF THE TEXT

2.1. Section Headings

According to the literature review, under the same conditions, the right-angle flexible hinge has the best effect, with a larger deformation than other types, which actually means that the structure has a very high sensitivity to external small excitations. Considering this significant characteristic, this paper selected the straight beam type flexible hinge in the design to take advantage of its superior sensitivity and deformation ability. As shown in Figure 1, the flexible hinge guidance mechanism has x and y directions with 4 flexible beams, which are symmetrically arranged and nested to allow for the addition of motion. There are 2 flexible beams on each side of the z direction, symmetrically arranged, so there are a total of 8 flexible beams.

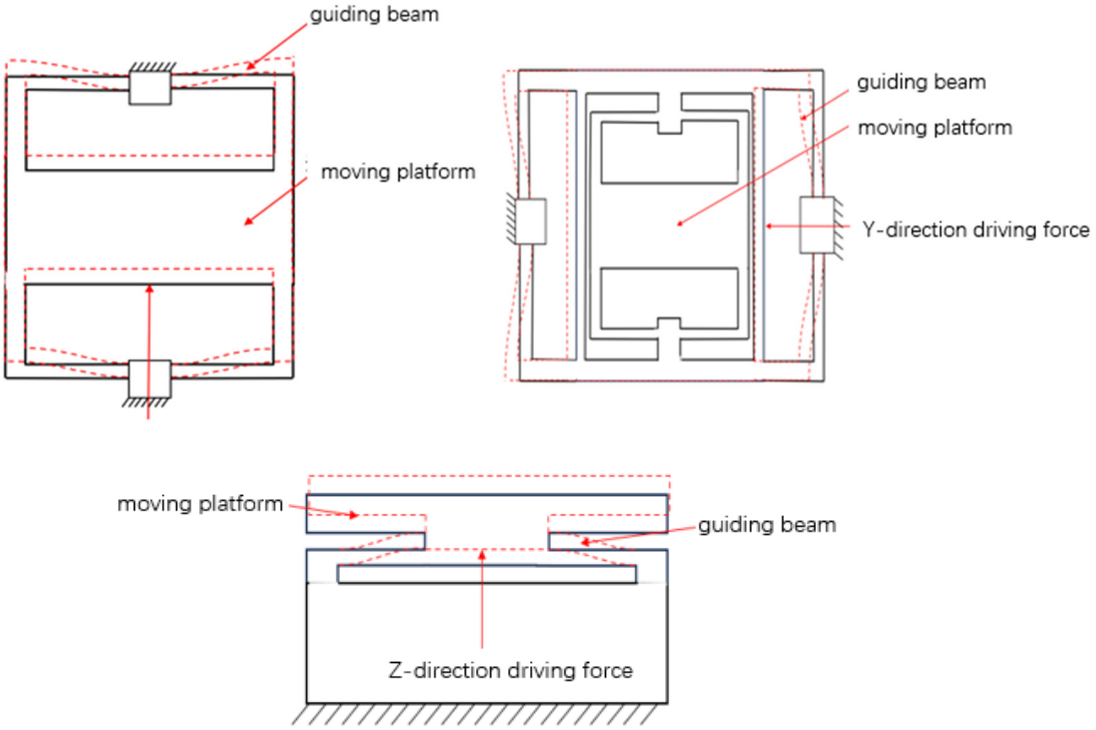

Figure 1. Compliant Flexure Hinge Guidance Mechanism Schematic

2.2. Design and Analysis of a Compliant Flexure Hinge Amplification Mechanism

Due to the limited output displacement of piezoelectric ceramics, which is only 30 μm, and the design requirement for a stroke of 50 μm × 50 μm × 20 μm, a compliant flexure hinge bridge-type amplification mechanism is introduced to effectively amplify the output displacement of the piezoelectric ceramic actuator. As shown in Figure 2, the bridge-type amplification mechanism, with

piezoelectric ceramics installed at its center, efficiently converts horizontal displacement into vertical displacement. Its symmetrical design not only achieves a relatively high amplification ratio but also effectively avoids issues related to lateral displacement. The schematic diagram of this mechanism is depicted in Figure 2.

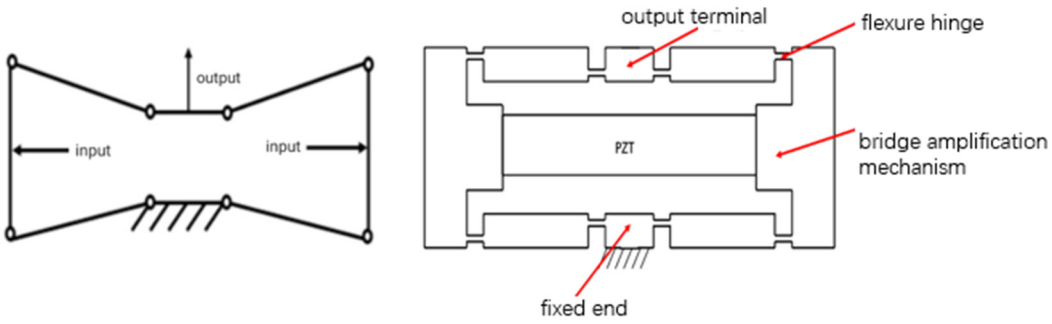

Figure 2. Schematic Diagram of a Compliant Flexure Hinge Amplification Mechanism

2.3. Integrated Structural Design

The internal structure design of this nano-positioning platform is depicted in Figure 3. It comprises four bridge-type amplification mechanisms, with one each for the x and y directions, and two symmetrical bridge-type amplification mechanisms for the z direction. To accommodate the preloading of piezoelectric ceramics, the bridge-type amplification mechanisms for the x and y directions differ from those for the z direction; the x and y direction mechanisms feature convex bridges, while the z direction mechanisms feature concave bridges. The overall encapsulation diagram is shown in Figure 3, with piezoelectric ceramics installed at the center of the bridge-type amplification mechanisms, generating a horizontal outward input displacement. This displacement is amplified by the bridge-type amplification mechanism, resulting in a magnified displacement that pulls or pushes the moving platform, thereby achieving the desired positioning effect and meeting the design specifications.

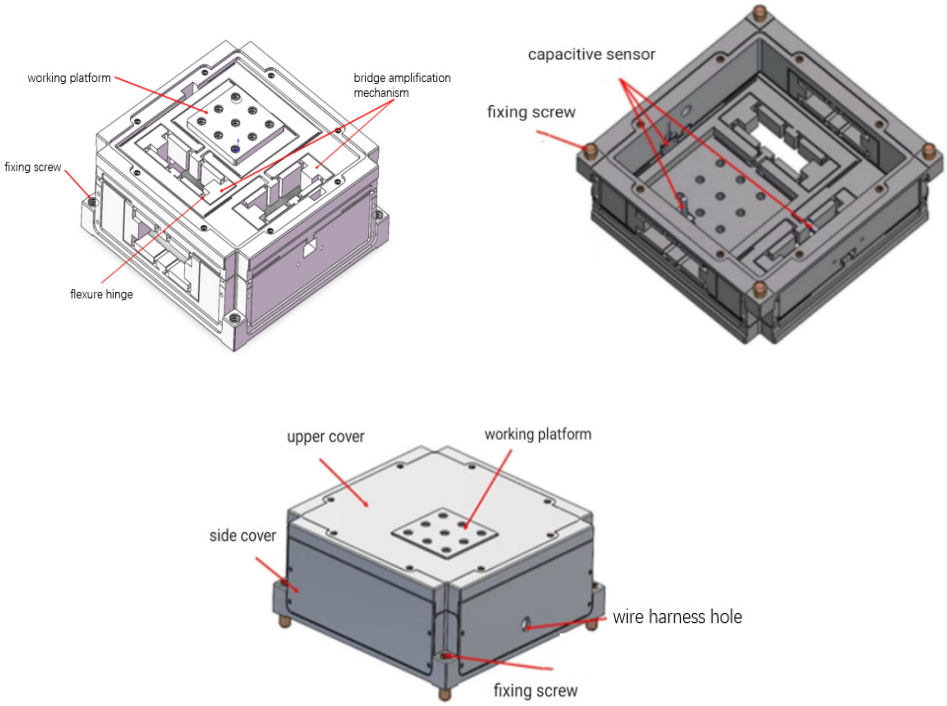

Figure 3. ntegrated Structural

3. THEORETICAL MODELING AND ANALYSIS

3.1. Static Mechanics Modeling

The equivalent modeling of the bridge-type amplification structure, as depicted in Figure 4, comprises a fixed block, an output block, two translational rods, four connecting beams, and eight compliant hinges. These components operate in concert such that upon the introduction of two equal input displacements at the input end, these displacements are amplified by the bridge mechanism, resulting in two correspondingly amplified output displacements at the output block.

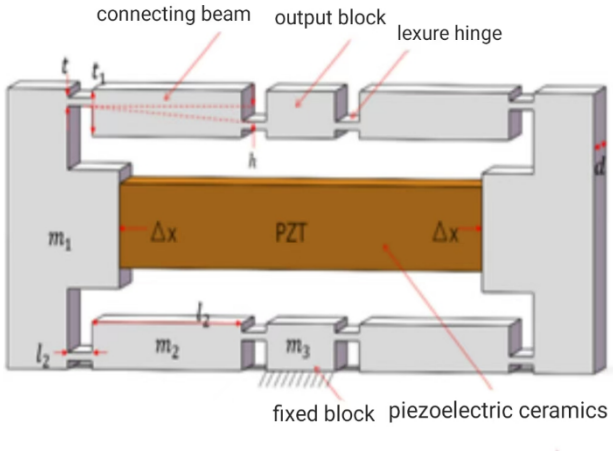

Figure 4. Bridge-Type Displacement Amplification Mechanism

t represents the thickness of the flexible hinge, t_1 denotes the thickness of the connecting beam, d signifies the width of the amplification mechanism, l_1 l_2 indicates the length of both the flexible hinge and the connecting beam, h is the spacing between flexible hinges, $m_1 m_2 m_3$ refers to the mass of the connecting beam, and Δx is the actuator displacement.

1. Euler-Bernoulli Beam Model

According to Figure 4, when performing static analysis on the bridge amplification mechanism, the specific part of the structure shown in Figure 5 is taken as the research object. Corresponding force equations are set for the connecting beam and flexible hinge.

$$F_A = f_B = f_x = f_{PZT} \quad (1)$$

$$2M_r = f_x h \quad (2)$$

In the above calculation equations, f_A and f_B are the distributed forces in the horizontal direction on the connecting beam; f_x is the tensile force on the flexible hinge; M_r is the rotational moment on the flexible hinge; f_{PZT} is the input force of the piezoelectric ceramic.

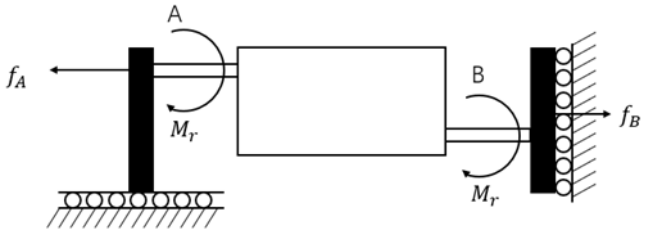

Figure 5. Euler-Bernoulli Beam Model

Referring to the principle of energy conservation, the work done by the force f_{PZT} is transformed into the bending potential energy of the flexible hinge under bending action and the tensile deformation energy under tensile action.

$$\frac{1}{2}f_{PZT}\Delta x = 2\int_0^{l_1}\frac{f_x^2(x)}{2EA(x)}dx + 2l\int_0^{l_1}\frac{M_r^2(x)}{2EI(x)}dx \tag{3}$$

In equation (3):Δx is the input displacement variable; $M_r(x)$is the rotational moment on the flexible hinge;$f_x(x)$ is the axially distributed force on the flexible hinge; $\mathrm{A(x)}$and $\mathrm{l}(x)$are the cross-sectional area and the moment of inertia of the flexible hinge; E is the modulus of elasticity. Referencing Hooke's law, it can be concluded that

$$f_x = K_{l_1}\Delta l_1 \tag{4}$$

In equation (4): f_x is the tensile force on the flexible hinge; K_{l_1}, $\Delta \mathrm{l}_1$and are the effective stiffness of the flexible hinge under tensile action and the elongation of the axial action.

Substituting equation (4) into equation (3) and calculating the integral, the axial input displacement of the bridge amplification mechanism is obtained as

$$\Delta \mathrm{x} = \left\{\frac{2}{\mathrm{K_{l_1}}} + \frac{\mathrm{h}^2}{2\mathrm{K_{\theta_1}}}\right\}\mathrm{f_x} \tag{5}$$

In equation (5):K_{θ_1} is the rotational stiffness of the flexible hinge under mechanical action.

Using Euler-Bernoulli beam theory to calculate the deflection of the bent beam as the output displacement $\Delta \mathrm{y}$, that is

$$\Delta \mathrm{y} = 2\iint \frac{\mathrm{M_{r(x)}}}{\mathrm{E_1 I(x)}}\mathrm{d^2x} + \int_0^{\mathrm{l1}}\int_0^{\mathrm{l2}}\frac{\mathrm{M_r(u)}}{\mathrm{E_1 I(u)}}\mathrm{d_u}\,dx \tag{6}$$

In equation (6): E_1 is the corrected modulus of elasticity.

Integrating equation (6) to obtain the output displacement as

$$\Delta \mathrm{y} = \frac{(\mathrm{l_1}+\mathrm{l_2})\mathrm{h}}{2\mathrm{K_{\theta_1}}}\mathrm{f_x} \tag{7}$$

In equation (7): l_1 and l_2 are the lengths of the flexible hinge and connecting beam, respectively.

Therefore, by combining equations (5) and (7), the amplification ratio of the Euler-Bernoulli beam model is calculated as

$$R_{amp1} = \frac{K_{l_1}h(l_1+l_2)}{4K_{\theta_1}+K_{l_1}h^2} \tag{8}$$

2.Euler-Bernoulli Beam Model Including Bending Deformation of Connecting Beam

Including the bending deformation of the connecting beam, the work done by the input force f_{PZT} becomes the bending potential energy of the flexible hinge and connecting beam under bending action and the bending deformation energy under tensile action. The output displacement of the bridge amplification mechanism is calculated as

$$\Delta x = \left\{ \frac{2}{K_{l_1}} + \frac{1}{K_{l_2}} + \frac{h^2}{2K_{\theta_1}} + \frac{h^2}{4K_{\theta_2}} \right\} fx \tag{9}$$

In equation (9), K_{θ_1} and K_{θ_2} represent the rotational stiffness and tensile stiffness of the connecting beam under mechanical action, respectively. According to the stiffness matrix, the values of K_{l_1} K_{θ_1} K_{θ_2} and K_{l_2} are calculated sequentially as follows [8]:

$$\begin{cases} K_{l_1} = \dfrac{E_1}{l_1} dt \\ K_{\theta_1} = \dfrac{E_1}{12 l_1} dt \\ K_{l_2} = \dfrac{E}{l_2} dt_1 \\ K_{\theta_2} = \dfrac{E}{12 l_2} dt_1^3 \end{cases} \tag{10}$$

In equation (10): d is the width of the flexible hinge; t is the thickness of the flexible hinge.

When d >10t, the modulus of elasticity E should be corrected to E_1 [8], that is

$$E_1 = \frac{E}{1 - v^2} E_1 = \frac{E}{1 - v^2} \tag{11}$$

In equation (11): v is Poisson's ratio.

The sum of the deflection of the flexible hinge and connecting beam is the output displacement Δy of the bridge amplification mechanism

$$\Delta y = 2 \iint \frac{M_r(x)}{E_1 I(x)} d^2x + \iint_{00}^{l_2 l_1} \frac{M_r(u)}{E_1 I(u)} du dx + \int_0^{l_2} \left[\int_0^x \frac{M_r(u)}{EI(x)} du \right] dx \tag{12}$$

Integrating equation (12) to obtain the output displacement micro as

$$\Delta y = \left[\frac{(l_1 + l_2)h}{2K_{\theta_1}} + \frac{l_2 h}{4K_{\theta_1}} \right] f_x \tag{13}$$

Combining equations (5) and (13), the amplification ratio of the Euler-Bernoulli model including the deformation of the connecting beam is calculated as

$$R_{amp2} = \frac{\dfrac{(l_1 + l_2)h}{2K_{\theta_1}} + \dfrac{l_2 h}{4K_{\theta_2}}}{\dfrac{2}{K_{l_1}} + \dfrac{1}{K_{l_2}} + \dfrac{h^2}{2K\theta_1} + \dfrac{h^2}{4K_{\theta_2}}} \tag{14}$$

3.Two-Degree-of-Freedom Beam Model

The bridge-type amplification mechanism is simplified into the linkage mechanism [9]as shown in Figure 6,Δy is the output displacement, f_N is the tensile force on the connecting beam, $\alpha$is the angle between the rod AB and the horizontal line before deformation, and α' is the angle between the rod AB and the horizontal line after deformation.$\Delta\alpha = \alpha - \alpha'$

Under the action of the input force, the mechanism undergoes a transformation from the solid line position to the dashed line position. During this deformation process, the rotation centers of the flexible hinges at both ends of the connecting beam of the bridge amplification mechanism move from the initial points A and B to new points A1 and B1. At the same time, due to this deformation, the horizontal angleα of the rod AB also changes accordingly, which is α' .

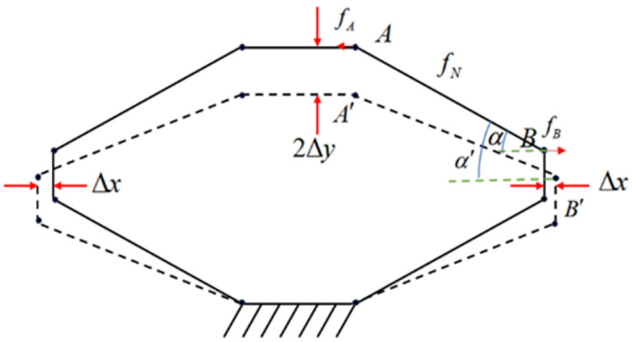

Figure 6. Simplified diagram of the bridge mechanism

According to equation (1), referring to Figure 6, the force and moment operation equations are established at the moving A end of the connecting rod

$$f_x h = 2M_r = 2K_{\theta_1}\Delta\alpha \tag{15}$$

$$f_N = \frac{f_x}{\cos\alpha} = K_{l_1}\Delta l_1 \tag{16}$$

Referring to the principle of virtual work, the energy operation equation is established [10]

$$f_x\Delta x = f_N\Delta l_1 + 2M_r\Delta\alpha \tag{17}$$

Combining equations (15) to (17), the axial displacementΔx of the bridge amplification mechanism is calculated as

$$\Delta x = \frac{2K_{\theta_1} + K_{l_1}h^2\cos^2\alpha}{2K_{\theta_1}K_{l_1}\cos^2\alpha}f_x \tag{18}$$

According to Figure 6, it can be obtained

$$l_y = l_{AB}\sin\alpha \tag{19}$$

In equation (19): l_{AB} is the shortest distance between points A and B.

Solving equation (19) for the complete differential to obtain

$$\mathrm{dl_y} = \mathrm{l_{AB}} \cos\alpha \, d\alpha + \sin\alpha \mathrm{d}\, \mathrm{l_{AB}} \tag{20}$$

Replacing the differential with a small increment to obtain

$$\Delta \mathrm{y} = \mathrm{l_{AB}} \cos\Delta\alpha + \sin\alpha \Delta\, \mathrm{l_{AB}} \tag{21}$$

Calculating and from equations (15) and (16),$\Delta\alpha$ and $\Delta \mathrm{l}_1$ substituting them into equation (21) to obtain

$$\Delta \mathrm{y} = \frac{\mathrm{K_{l_1}} \mathrm{l_{AB}} \mathrm{h} \cos\alpha + 2\mathrm{K_{\theta_1}} \tan\alpha}{2\mathrm{K_{\theta_1}} \mathrm{K_{l_1}}} \tag{22}$$

Finally, combining equations (18) and (22), the amplification ratio of the two-degree-of-freedom model is calculated as

$$R_{amp3} = \frac{K_{l_1} l_{AB} h \cos\alpha + 2K_{\theta_1} \tan\alpha}{2K_{\theta_1} + K_{l_1} h^2 cos^2\alpha} \tag{23}$$

3.2. Dynamic Modeling

When further exploring the dynamic characteristics of the bridge mechanism, considering its unique output characteristics, that is, it has only one degree of freedom in the y direction, we choose the input displacement as the key generalized coordinate q for study. Referring to the mechanism model shown in Figure 4, we can further analyze and describe the system kinetic energy of the bridge amplification mechanism.

$$\mathrm{T} = \frac{1}{2}\mathrm{m_3 d^2} + 2 \times \frac{1}{2}\mathrm{m_1}\left[\left(\frac{\mathrm{q}}{2}\right)^2 + \left(\frac{\mathrm{d}}{2}\right)^2\right] + 4 \times \frac{1}{2} \times \frac{1}{12}\mathrm{m_2 l_{AB}^2 \alpha^2} +$$
$$2 \times \frac{1}{2}\mathrm{m_2}\left[\left(\frac{\mathrm{q}}{4}\right)^2 + \left(\frac{\mathrm{d}}{4}\right)^2\right] + 2 \times \frac{1}{2}\mathrm{m_2}\left[\left(\frac{\mathrm{q}}{4}\right)^2 + \left(\frac{3\mathrm{d}}{4}\right)^2\right] \tag{24}$$

In equation (24):q is the output displacement of the mechanism, and d is the input displacement of the mechanism, obtained from equation (23) $\mathrm{d} = \mathrm{R_{amp2}} \mathrm{q}$.

According to Lagrange's equation [11], the equivalent mass M and equivalent stiffness K of the bridge amplification mechanism are

$$M = \frac{1}{4} m_1 \left(1 + R_{amp2}^2\right) + \frac{1}{4} m_2 \left(1 + \frac{16}{3} R_{amp2}^2\right) + \frac{1}{2} m_3 R_{amp2}^2 \tag{25}$$

$$\mathrm{K} = \frac{2\mathrm{R_{amp2}^2 K_{\theta_1}}}{\mathrm{l_{AB}^2}} \tag{26}$$

The natural frequency of the bridge amplification mechanism is calculated as

$$\mathrm{f} = \frac{1}{2\pi}\sqrt{\frac{\mathrm{K}}{\mathrm{M}}} \tag{27}$$

4. AMPLIFICATION RATIO ANALYSIS

Flexible hinges are a type of precision mechanical structure that accurately transmits displacement and torque through minor deformations. The material's flexibility, stiffness, strength, and the ratio of Young's modulus are crucial to the performance of the micro-positioning platform. The ratio of strength to Young's modulus is key when selecting materials; the higher the ratio, the more flexible and stronger the material. After a series of comparative calculations, we chose AL7075-T6 as the material for the micro-positioning platform and conducted finite element simulation.

4.1. Finite Element Analysis of Micro-motion Platform

Given that the maximum displacement limit of the piezoelectric ceramic actuator set in this paper is 30 μm, when analyzing the displacement characteristics of the micro-motion platform, we need to ensure that each side of the bridge amplification mechanism receives an input displacement of 15 μm. The displacement cloud map is shown in Figure 7.

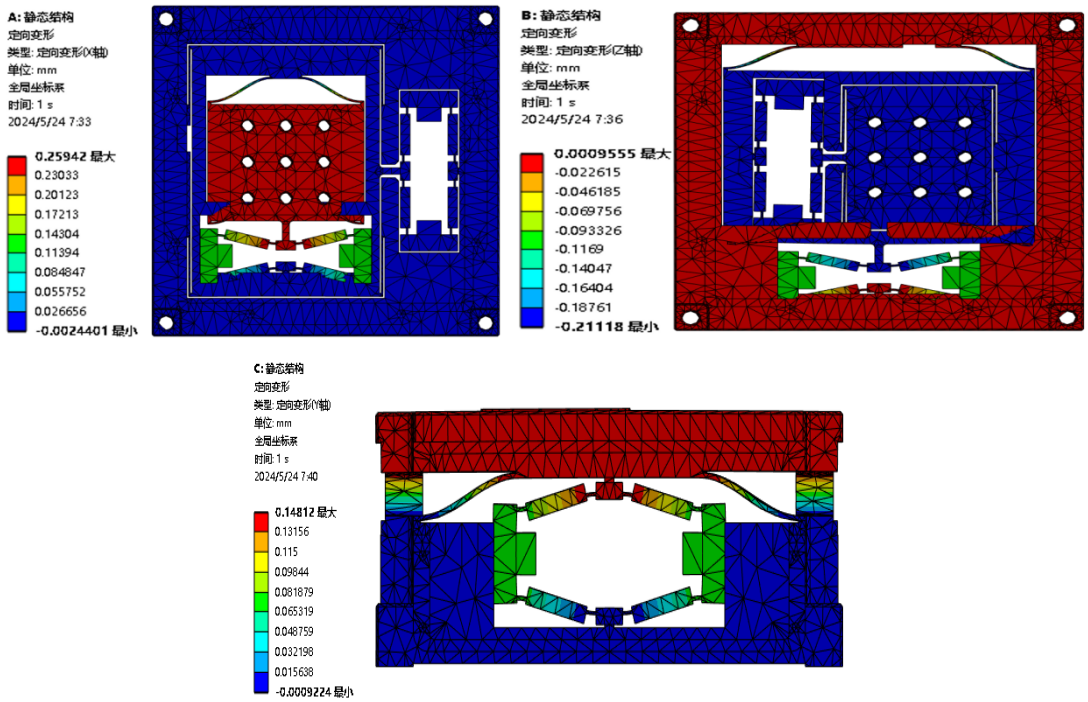

Figure 7. Displacement cloud map of the dynamic platform

hen evaluating the output amplification ratio of the dynamic platform in the negative x and y directions, 15 μm of outward input displacement is applied to both sides of the bridge amplification mechanism. The simulated displacement cloud map is shown in Figures 7(a) and 7(b). The maximum output displacement of the dynamic platform in the negative x direction is 259.42 μm, and the input displacement is 30 μm, with a displacement amplification factor of 8.65.The maximum output displacement of the dynamic platform in the negative y direction is 211.18 μm, and the input displacement is 30 μm, with a displacement amplification factor of 7.04.

When evaluating the output amplification ratio of the dynamic platform in the positive z direction, 15 μm of outward input displacement is applied to both sides of the bridge amplification mechanism. The simulated displacement cloud map is shown in Figure 7(c), and the maximum output displacement of the dynamic platform in the positive z direction is 148.12 μm, with an input displacement of 30 μm, resulting in a displacement amplification factor of 4.94.

4.2. Stiffness Analysis

Stiffness is defined as the ratio of unit force to the displacement produced by the unit force in a specific direction. To comprehensively evaluate the platform's stiffness characteristics in the x, y, and z directions, we will use finite element analysis software for in-depth analysis.

When conducting stiffness analysis in the x, y, and z directions, a 10 N force is applied to the nodes of the bridge mechanism in the x, y, and z directions, respectively. This method allows us to accurately obtain the platform's stiffness performance in each direction. The finite element analysis results are shown in Figure 8.

It can be seen from the figure that when a 10 N force is applied to the platform, the platform produces corresponding output displacements in the x, y, and z directions. Using the stiffness calculation formula, the output stiffness values of the platform moving along the x, y, and z directions are determined to be 1.04 N/μm, 1.78 N/μm, and 2.78 N/μm, respectively.

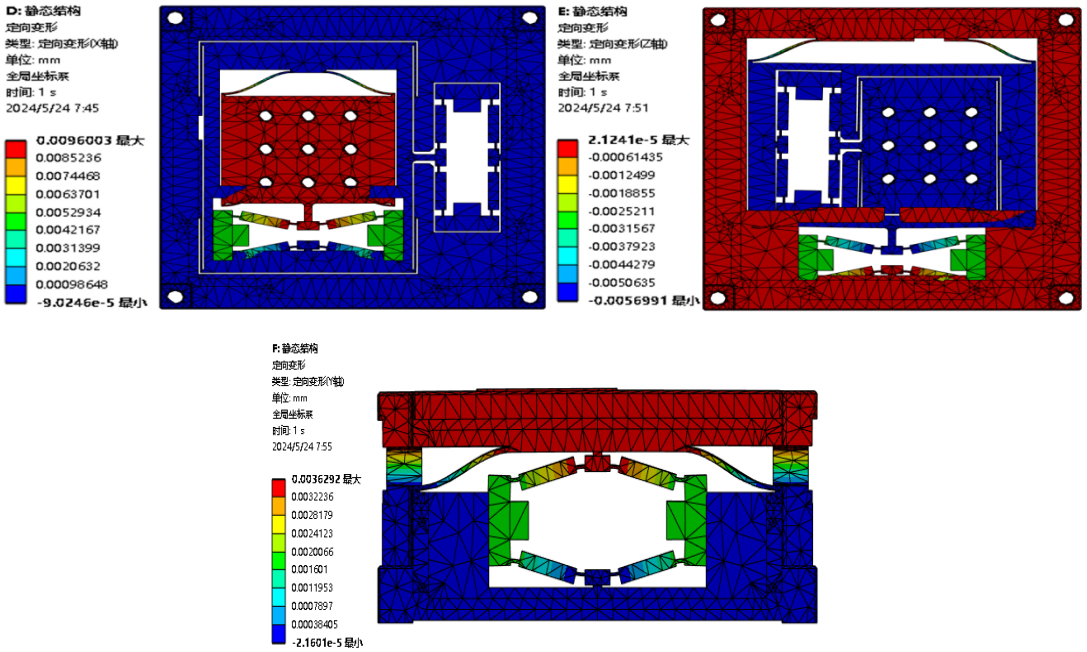

Figure 8. Stiffness analysis displacement cloud map

4.3. Stress Analysis

When constructing the micro-motion platform, we chose aluminum alloy 7075 as the main material, which has a permissible stress of up to 503 MPa. Given that the flexible hinges are usually the parts that bear the maximum stress during the operation of the micro-motion platform, exceeding the permissible stress can cause structural damage. Therefore, we need to analyze the actual stress in each direction of motion when the platform reaches its maximum output displacement using finite element simulation.

As shown in Figure 9, these are the stress cloud maps of the dynamic platform's output in three directions. It can be seen from the figure that the maximum stress generated when the platform moves in the x, y, and z directions is 123.3 MPa, 122.9 MPa, and 101.27 MPa, respectively. The simulated values in these three directions are all much lower than the maximum permissible stress of the selected material, aluminum alloy 7075, indicating that the movement of the micro-motion platform has always been within the elastic stage of the maximum permissible stress of the selected material.

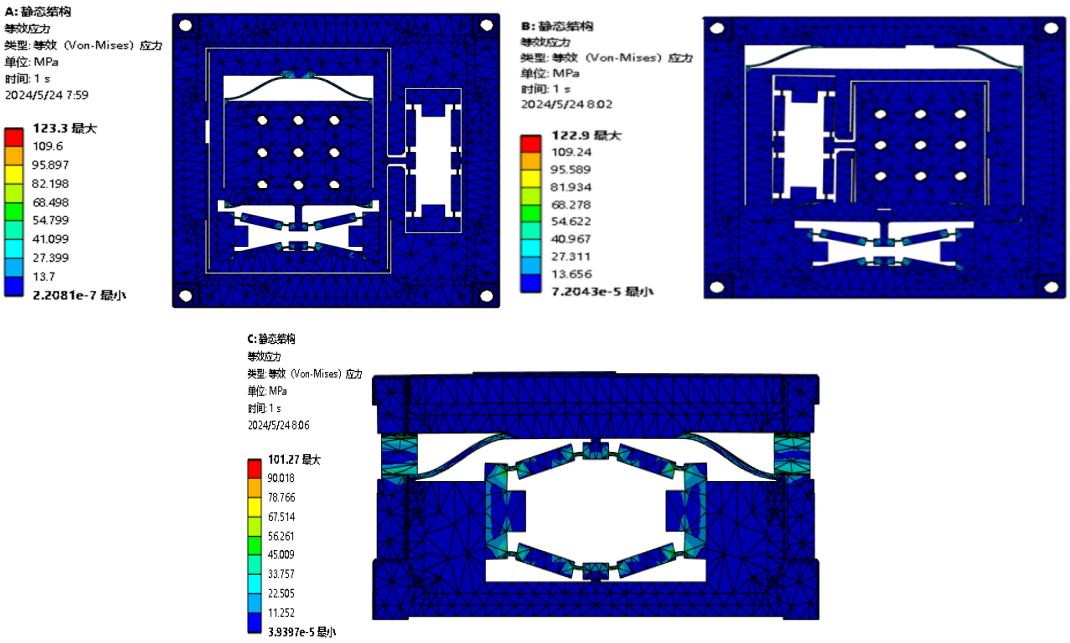

Figure 9. Stress cloud map of the dynamic platform

4.4. Modal Analysis

Resonance phenomena pose a threat to the motion accuracy of the micro-motion platform and can even cause structural damage in extreme cases. Therefore, preventing resonance is a key part of the work. To effectively predict and avoid resonance, we can use modal analysis technology to conduct finite element simulation studies on the platform's vibration characteristics, thereby accurately obtaining the natural frequencies and corresponding vibration modes of the three-degree-of-freedom nanopositioning platform, ensuring the stable operation of the platform.

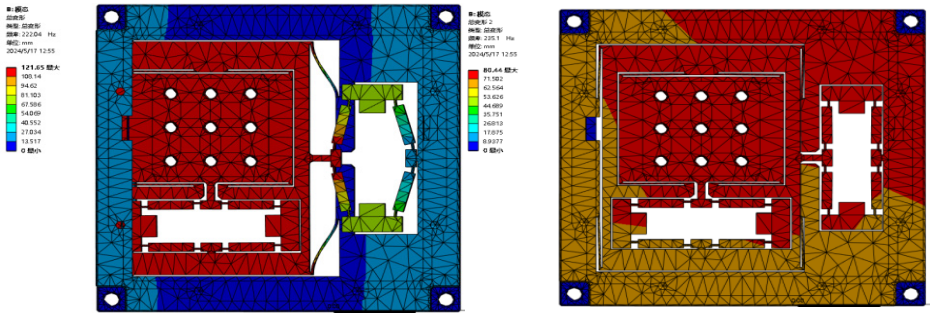

Figure 10. Modal vibration cloud map

The analysis results are shown in Figure 10. It can be seen that the main motion forms of the three-degree-of-freedom nanopositioning platform are the movements in the x, y, and z directions and their natural frequencies.

5. SUMMARY

This paper designs a three-degree-of-freedom nanopositioning platform in the X, Y, and Z directions, with the overall size of the platform being 100 mm×100 mm×36 mm. The platform structure is compact and can achieve three-degree-of-freedom movement. By installing piezoelectric ceramics in the middle of the bridge amplification mechanism, it produces a horizontal outward input displacement, which is amplified by the bridge amplification mechanism to pull or push the dynamic platform, thereby achieving positioning effects and meeting design requirements. Using ANSYS for finite element simulation, the maximum output displacement of the micro-motion platform along the

negative x direction is 259.42 μm, along the negative y direction is 211.18 μm, and along the positive z direction is 148.12 μm, with amplification ratios of 8.64, 7.04, and 4.94, respectively. The consistency between theoretical analysis and simulation analysis results is verified.

CONFLICTS OF INTEREST

The authors declare that they have no conflict of interest.

ACKNOWLEDGMENTS

Tianjin College Students' innovation and entrepreneurship training program(202310066107),Tianjin Education Commission scientific research plan project (2023KJ189), Tianjin metrology technology project (2024TJMT048),Tianjin Research Innovation Project for Postgraduate Students (2022SK YZ016).

REFERENCES

[1] Olaniyan T, Faisal N ,Njuguna J . Recent Developments in Mechanical Ultraprecision Machining for Nano/Micro Device Manufacturing [J]. Micromachines, 2024, 15 (8): 1030-1030.

[2] Hongbo Lan, Yucheng Ding et al. Review of the wafer stage for nanoimprint lithography[J]. Elsevier Bv, 2007, 84(4): 684-688.

[3] Yuan H, Yimin W, Shichao J , et al. Design and Analysis of a Microgripper with Three-Stage Amplification Mechanism for Micromanipulation [J]. Micromachines, 2022, 13 (3): 366-366.

[4] Sheng S,Chen L, Schust J , et al. Control of Surface Plasmon Propagation and Terahertz Near-Field Waveforms in a Scanning Tunneling Microscope. [J]. Nano letters, 2024.

[5] Zhou Liping, Zhang Quan, Sun Zhijun. Precision Positioning of a 3-PRR Planar Parallel Manipulator Driven by Linear Ultrasonic Motors Based on Machine Vision [J]. Journal of Mechanical Engineering, 2014, 50 (19): 18-23.

[6] Meng Fancun, Zhang Shijun, Zhang Teng, et al. Design and simulation of differential micro-displacement amplification platform with three degrees of freedom [J]. Machine Design and Manufacturing Engineering, 2023, 52 (01): 18-22.

[7] Tian Yanling, Zhang Dawei, Yan Bing. Kinematic Characteristics of a 3-DOF Micropositioning Table for Precision Grinding [J]. Journal of Tianjin University, 2006, (07): 777-782.

[8] Wang Baoxing, Meng Gang, et al. Design and analysis of a 3-PPP compliant parallel micro-positioning stage [J]. Journal of Beijing University of Aeronautics and Astronautics, 2020, 46(04): 798-807.

[9] Shen Jianying, Zhang Haijun. Calculation, analysis and experimental verification of the magnification ratio for novel bridge-type mechanism [J]. Chinese Journal of Scientific Instrument, 2015, 36(08): 1877-1883.

[10] Ma Jinyu, Yu Shengdong, et al. Design and Motion Control of Piezo-driven Puncture Micromanipulation Mechanism [J]. Transactions of the Chinese Society for Agricultural Machinery, 2021, 52(09): 417-426.

[11] Song Shuaiguan, Yang Yiling, et al. Design and Analysis of a Piezoelectric Compliant X-Y Micro Gripper [J]. Journal of Vibration and Shock, 2022, 41(10): 154-161.